LIQUID METAL HEAT TRANSFER UNDER LOW PECLET NUMBER CONDITIONS

Hiroyasu Mochizuki
Research Institute of Nuclear Engineering, University of Fukui,
1-2-4 Kanawa-cho, Tsuruga, Fukui, 914-0055, Japan
mochizki@u-fukui.ac.jp

ABSTRACT

This paper describes the liquid metal heat transfer in heat exchangers under low flow rate conditions, i.e., low Péclet number conditions. Measured data from some experiments indicate that heat transfer coefficients to liquid metals under the low Péclet number conditions are much lower than what are predicted by the theoretically calculated values. In the present study, an IHX of the "Monju" reactor is calculated using a Computational Fluid Dynamics (CFD) code. The calculated temperatures in the IHX are compared with the measured results using the IHX in the "Monju" reactor, and good agreement has been obtained. The calculated results show that the heat transfer in the lower plenum of the IHX is considerably large when the flow rate is low such as natural circulation condition. Inspired by the CFD calculation, the same IHX is analyzed using a one-dimensional system code with a model based on three, separated countercurrent heat exchanger models: one heat exchanger models heat transfer in the tube bank, while the upper and lower plena are modeled as two heat exchangers with a single heat transfer tube. The Nusselt number, as a function of the Péclet number, calculated from measured temperature and flow rate data in a 50MW experimental facility is correctly reproduced by the calculation with the same heat transfer correlation by Seban & Shimazaki. Finally it is clarified that the deviation is a superficial phenomenon which is caused by the heat transfer in the plena of the heat exchanger.

KEYWORDS
Degradation of heat transfer, liquid metal, heat exchanger, Nusselt number, Low Péclet number

1. INTRODUCTION

This paper describes the liquid metal heat transfer in heat exchangers under low flow rate conditions, i.e., low Péclet number conditions. For low Pe number, there exists a well-known anomaly: in certain experiments, the experimental Nusselt number is much lower than what is theoretically expected. Therefore the objective of the present research is to clarify the cause of the anomaly degraded heat transfer coefficient.

Heat transfer to liquid metals has been studied by many researchers using various kinds of liquid metals. Lyon [1] derived the correlation taking into account the sodium velocity distribution in a pipe heated with a constant heat flux. Seban and Shimazaki [2] proposed the heat transfer correlation in a pipe by analyzing heat transfer under the condition of constant wall temperature. The same correlation was proposed by Subbotin et al. [3] based on the experiment using liquid sodium. Lubarsky and Kaufman [4] reviewed a large number of experimental data about the heat transfer of liquid metals and proposed their best fit correlation. Most recently, Pacio et al. [5] also reviewed past experimental data and correlations about heat transfer of liquid metals in pipes. Above mentioned important correlations are listed below;

$$Nu = 7 + 0.025\,Pe^{0.8} \quad \text{by Lyon} \tag{1},$$

$$Nu = 5 + 0.025\,Pe^{0.8} \quad \text{by Seban and Shimazaki} \tag{2},$$

$$Nu = 0.625\,Pe^{0.4} \quad \text{by Lubarsky and Kaufman} \tag{3}.$$

The Nusselt number measured using an intermediate heat exchanger (IHX) of the 50 MW Steam Generator Facility (50MW SG) decreased with decreasing Pe number for low flow rate conditions although the Nu number based on the theory shows almost constant under the low Pe number conditions as shown in reference [6]. Similar data can be seen in the old literature by Lubarsky and Kaufman. These are data by Johnson et al. [7]. Until now, it was a question whether or not these data tendencies show an actual characteristics or are caused by experimental error. The heat transfer coefficient measured using the IHX at 50 MW SG under steady state was evaluated using the following equations;

$$Q = \frac{\Delta T_{l,m}}{R} \tag{4},$$

$$Q = m_p Cp_p\left(T_{pi} - T_{po}\right) = m_s Cp_s\left(T_{so} - T_{si}\right) \tag{5},$$

$$R = \frac{1}{\pi NL}\left(\frac{1}{d_o h_p} + \frac{1}{d_i h_s} + \frac{1}{2k_t}\ln\left(\frac{d_o}{d_i}\right) + \frac{1}{d_o h_{fp}} + \frac{1}{d_i h_{fs}}\right) \tag{6},$$

$$\Delta T_{lm} = \frac{\Delta T_1 - \Delta T_2}{\ln\left(\frac{\Delta T_1}{\Delta T_2}\right)} = \frac{\left(T_{pi} - T_{so}\right) - \left(T_{po} - T_{si}\right)}{\ln\left(\frac{T_{pi} - T_{so}}{T_{po} - T_{si}}\right)} \tag{7},$$

$$d_o h_p \Delta T_p = d_i h_s \Delta T_s, \qquad (\Delta T_k = c\,\mathrm{Re}_k^{0.8},\ k{=}p \text{ or } s) \tag{8}.$$

We have calculated temperature data and flow rate data for Eqs. from (4) to (7) in order to evaluate R and ΔT_{lm}. In this process, we have to assume h_{fp} and h_{fs} based on our experience. Since we have to calculate the ration of h_p and h_s using Eq. (8), the individual heat transfer coefficient is calculated.

A project has been launched in order to study the thermal-hydraulics of the IHX of the "Monju" reactor which is a prototype liquid sodium cooled fast breeder reactor. Since the measurement of temperature distribution in the IHX was impossible, the establishment of the calculation method using a Computational Fluid Dynamics (CFD) code was thought as a kind of breakthrough to investigate the heat transfer in a heat exchanger. This investigation in the early stages suggested that the heat transfer in the lower plenum of the IHX between the primary (shell-side) and the secondary (tube-side) fluids becomes dominant as the flow rates on the primary and secondary sides decreased. Since the heat transfer area in the plenum is relatively small, it was commonly assumed that heat transfer could be neglected in the plena. However, the CFD analysis shows that the reality is opposite. Therefore, a numerical study of the heat transfer in the IHX is carried out using the one-dimensional system code NETFLOW++, inspired by the above CFD study. The IHX model is modified in order to simulate the heat transfer in the lower and the upper plena as well as the heat transfer tube region.

2. CFD ANALYSIS

2.1. Modeling

Although it was studied to create a one-piece model of the IHX at first, calculation meshes were too coarse to obtain an accurate result. Therefore, the IHX of the "Monju" reactor illustrated in **Fig. 1** is divided into

three models. These are: model-I: the primary side of the IHX; model-II: mainly the secondary side; and model-III for the heat transfer tube region on the primary and the secondary sides. Model-I consists of the inlet nozzle, flow distribution mechanism, windows, bellows region, primary outlet and the top part of the heat transfer tubes. Model-II consists of the center pipe, the lower plenum with the flow rectifier ring on the secondary side and a part of the primary side at the lower plenum region. Model-III consists of the heat transfer tubes on the primary (shell) and the secondary (tube) sides, and the rectifier plates on the primary side. If sector models can be applied for the model-III, the number of meshes can be drastically reduced. An important condition is whether or not the thermal hydraulic situation at the inlet windows of the shell is assumed as axisymmetric to calculate the heat transfer tube region with the sector model. Since the IHX of "Monju" has only one nozzle supplying the primary sodium into the shell, a confirmation of the uniformity of the flow distribution to the bank of heat transfer tubes is necessary. If the flow distribution is not uniform, the sector model cannot be adopted. The ANSYS CFX code is used to calculate the thermal hydraulics in the IHX. Major specifications of the IHX are listed in **Table 1** together with those of the IHX of 50MW SG.

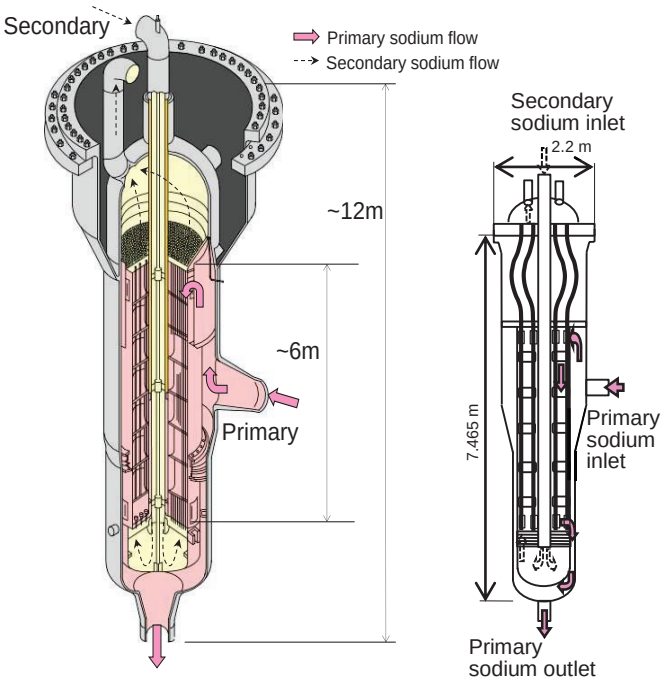

Figure 1. Schematics of IHXs of the "Monju" reactor (left) and 50MW SG Facility (right).

Table I. Specifications of the intermediate heat exchangers.

Items	Monju	50 MW SG
Capacity (MW)	238	50
Number of heat transfer tubes	3294	2044
Outside diameter of heat transfer tube (m)	0.0217	0.0159
Thickness of heat transfer tube (m)	0.0012	0.0012
Actual length	6.0	4.44
Effective heat transfer length in design (m)	4.86	3.90
Flow rate on secondary side (kg/s)	1038	222
Outside diameter of outer shroud (m)	2.184	1.560
Thickness of outer shroud (m)	0.025	0.0240
Outer diameter of inner shroud (m)	0.746	0.457
Inner diameter of inner shroud (m)	0.020	0.0143
Flow rate on primary side (kg/s)	1422	263
Total length (m)	Approx. 12	Approx. 9

2.2. Separated Models

Since the primary sodium is fed to the shell of the IHX through one nozzle welded on the shell and 6 windows are provided to distribute sodium to the heat transfer tube region on the primary side, a flow distribution mechanism is provided to obtain a uniform flow rate, as far as possible, for each inlet window. The flow distribution is controlled with small-diameter holes arranged in the annulus of the outer and inner shrouds as illustrated in **Fig. 2**. If the holes illustrated on the right of the Model-I are arranged uniformly, we have large amount of flow rate at the windows opposite to the inlet nozzle by the hydrodynamic reasons. Therefore, the arrangement of holes are not uniform. We have obtained information of the total area of the holes in the different domain corresponding to the window, and the total flow areas of the holes for every 60^{o} sectors containing one window are adjusted in the calculation model.

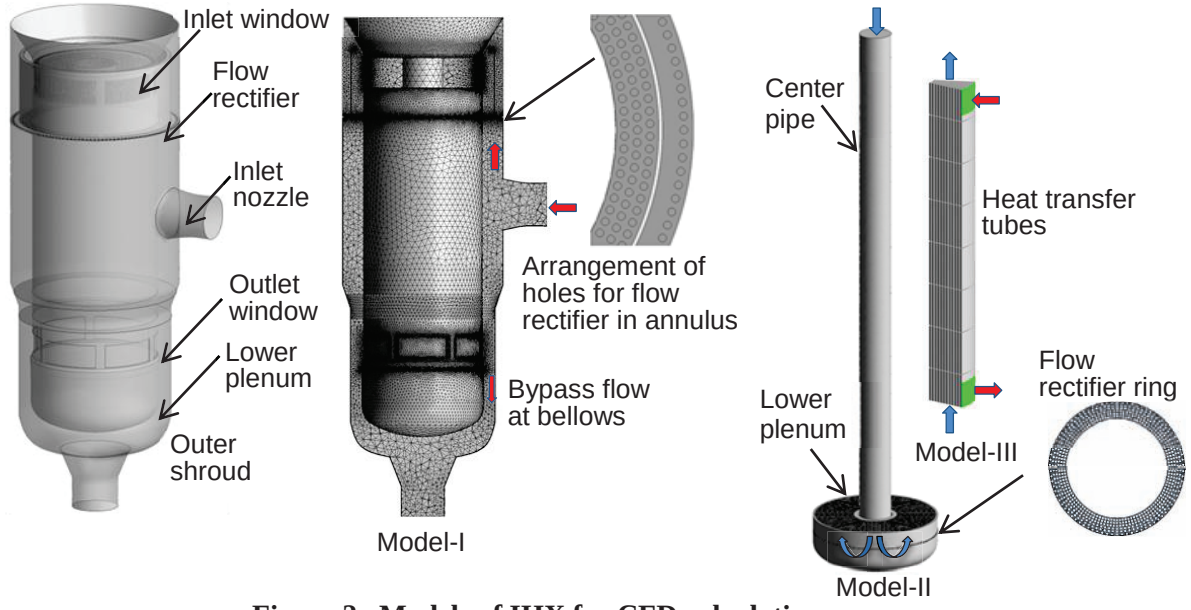

Figure 2. Models of IHX for CFD calculation.

Table II. Analysis conditions on the primary side.

CFD code	ANSYS CFX
Turbulent model, Convection term	Standard k-ε model, 2nd order up-wind differencing
Coolant and physical properties	Liquid metal sodium with Polynomial approximations
Inlet boundary conditions	Temperature at the inlet nozzle, Mass flow rate at the inlet nozzle Well-developed velocity and turbulence intensity
Outlet boundary condition	Pressure at 0.1 MPa
Wall surface conditions	Heat transfer coefficient from sodium to outside: 0.26 W/m^2 K (estimated by hand calculation) Outside temperature 25 ^{o}C
Gravitational acceleration	-9.806665 m/s^2
Buoyancy	Boussinesq approximation

General calculation conditions are listed in **Table II**. These models and calculation conditions are summarized in **Table III**. The thickness of the first layer in the boundary layer corresponds to y≈100, and a scalable wall function is applied. This wall function is an option of the code to escape from problems caused in refined meshes below y+ = 30, and it is applicable for the meshes with even y+ = 1. In terms of buoyancy, the Boussinesq approximation is used in all the calculation. In the calculation, the inlet flow rate and temperature and outlet pressure are given to the code. The calculated results are transferred to the other model. A bellows seal is provided between the outer and inner shrouds in order to absorb the thermal expansion difference between two shrouds. The bellows seal has small holes to drain the sodium during a standstill. Therefore, the approximately 2% of the primary mass flow rate is bypassed directly to the outlet nozzle direction. This condition should also be taken into account in the CDF calculation.

Table III. Calculation models using CFX code.

Items	Model-I	Model-II	Model-III
System	Primary	Secondary +primary at lower plenum	Primary and secondary coupled
Model range	Inlet nozzle - Window	Center pipe – heat transfer tube	Heat transfer tube
First layer height	3.15×10^{-4} m	2.4×10^{-4} m	3.15×10^{-4} m
Number of elements	12.8 million	11.7 million	5 million
Mesh configuration	Hexahedron- and tetrahedron	Hexahedron and tetrahedron	Hexahedron
Turbulence model	Standard k- ε with scalable wall function	Standard k- ε with scalable wall function	Standard k- ε with scalable wall function
Convection term	2nd order upwind	2nd order upwind	2nd order upwind
Buoyancy	Boussinesq approx.	Boussinesq approx.	Boussinesq approx.
Boundary conditions	Inlet flow rate and temperature, outlet pressure Well-developed velocity and turbulence intensity at the inlet	Inlet flow rate and temperature, outlet pressure Well-developed velocity and turbulence intensity at the inlet	Inlet flow rates and temperatures, outlet pressures Calculated results by Model-I and Model-II

2.3. Calculated Results

It was confirmed in advance using the Model-I with several layers of heat transfer tubes whether or not the flow distribution from every windows was uniform. As a result of the CFD calculation, the flow distribution from the window is almost uniform and the distribution is not changed when the number of layers of the heat transfer tubes exceeds 3. The flow rate discrepancy against the average flow rate from each window was in the range of ±4 %. The configuration of flow rectifier holes in the annulus was decided by the water test. The experimentally decided conditions were proven by the CFD analysis using the informed diameter and arrangement of holes. The calculated results are transferred to calculate the thermal-hydraulics on the primary side of the heat transfer tube using the Model-III.

The thermal-hydraulics on the secondary side is calculated using the Model-II and the lower part of the Model-I in order to calculate the heat transfer between the primary and the secondary flows at the lower plenum. Since this region does not contain any complex geometry, the full-sector model is adopted. The characteristics of the flow rectifying ring were checked beforehand. Discrepancy of flow rate for each heat

transfer tube layer from the average was in the range from -7% to +4 % for a wide flow rate range (100%, 48%, 10%, 3 % flow rate). The calculated results are transferred to calculate the thermal-hydraulics on the secondary side of the heat transfer tube using the Model-III.

The Model-III includes 7 rectifier plate regions on the primary side. These parts are modeled with the porous media. Thermal-hydraulics on the primary side was calculated beforehand using the model with the actual configuration of the heat transfer tubes and the plates in order to obtain proper local pressure loss coefficients. The porosities are evaluated taking into account the cross-sectional flow area and the structure area.

Temperature and velocity distributions in the IHX are calculated by a series of above mentioned calculations. **Fig. 3** shows an example of the distributions under the condition of the initial steady state at 45% thermal power. As you can see from this figure, the heat transfer between the primary and the secondary takes place at the lower part of the heat transfer tube. The lower plenum acts as a kind of heat exchanger too. The uniform flow rate distribution for the inlet of the heat transfer tube was applies as well. The temperature distributions on both sides had negligible effects.

When the reactor is scrammed and the heat transport systems are cooled with small flow rates at approximately 10% of the rated flow rates, the heat transfer region moves to downward as shown in **Fig. 4**. Temperatures around the IHX were measured at "Monju" during the turbine trip test. These are inlet and outlet temperatures on both sides, and shell outside temperatures. The temperatures on the shell reflect the temperature distribution inside the IHX. If the inside temperature distribution is not predicted properly, the temperatures on the shell are not accurate. The calculated result are compared with the measured results as listed in **Table IV**. These temperatures are predicted within the error of 5K. Therefore, it is concluded that the temperature distribution in the IHX is calculated properly using the CFD method. Furthermore, the CFD result suggests us that the heat transfer in the lower plenum should be taken into account under the low flow rate conditions.

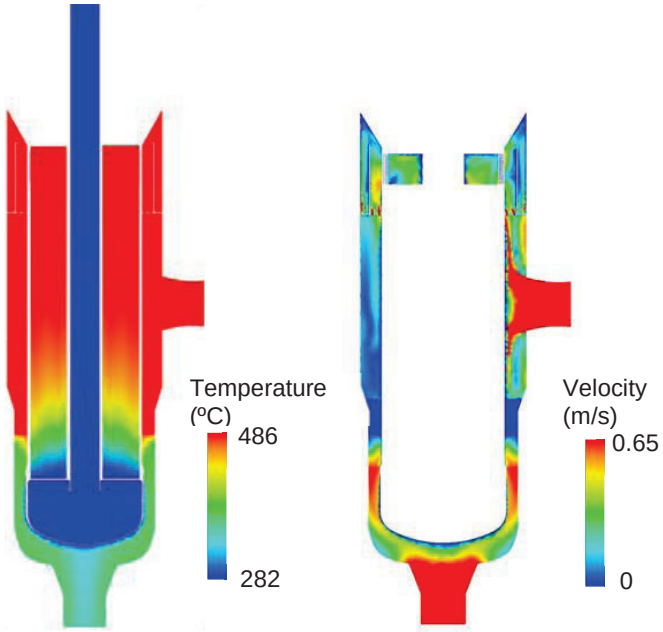

Figure 3. Temperature and velocity contour maps for the initial steady state (45% thermal power) for the coupled three model calculation.

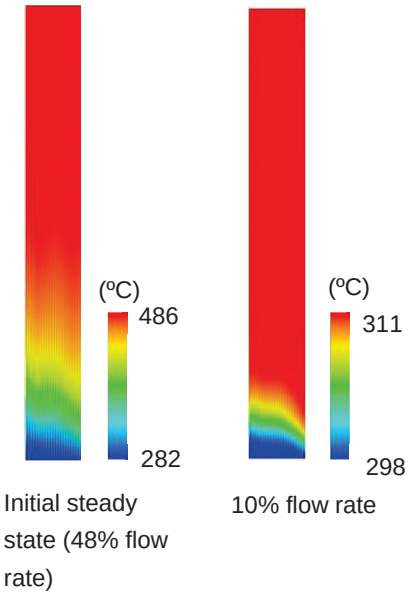

Figure 4. Temperature contour maps in the tube region for the initial steady state and the decay power condition.

Table IV. Comparison between calculated and measured results.

Item	48% flow rate condition		10% flow rate condition	
	Measured	Calculated	Measured	Calculated
Primary flow rate (kg/s)	690.4	Input	393.8	Input
Secondary flow rate (kg/s)	139.0	Input	77.7	Input
IHX primary inlet $T_{p,i}$(˚C)	486	Input	311	Input
IHX primary outlet $T_{p,o}$(˚C)	364	366.1	306	305.0
IHX secondary inlet $T_{s,i}$(˚C)	282	Input	298	Input
IHX secondary outlet $T_{s,o}$(˚C)	484	485.9	311	311.0
T_1 (˚C)	456	457.9	313	310.4
T_2 (˚C)	410	414.8	314	308.8

3. ONE-DIMENSIONAL ANALYSIS

Inspired by the CFD analysis, the thermal hydraulics in the same IHX is calculated using the one-dimensional system code NETFLOW++ with the model taking into account the heat transfer in plena as well as the heat transfer tube region. Up to now, the heat transfer in the plena were neglected in the most one-dimensional calculations. However, the IHX should be separated into a couple of parts, especially under the low flow rate conditions.

3.1. One-dimensional Calculation Model

One of heat transport systems on the secondary side of "Monju" is modeled. The IHX is separated into three countercurrent type heat exchangers, i.e., lower and upper plena, and the heat transfer tube region, as shown in **Fig. 5**. Since the heat transfer in the lower plenum cannot be neglected, the IHX should be divided into at least two heat exchangers in order to evaluate the heat transfer coefficient in the heat transfer tube. In regard to the upper plenum, since the contribution to the heat transfer coefficient is not clear, this part is also modeled as a heat exchanger.

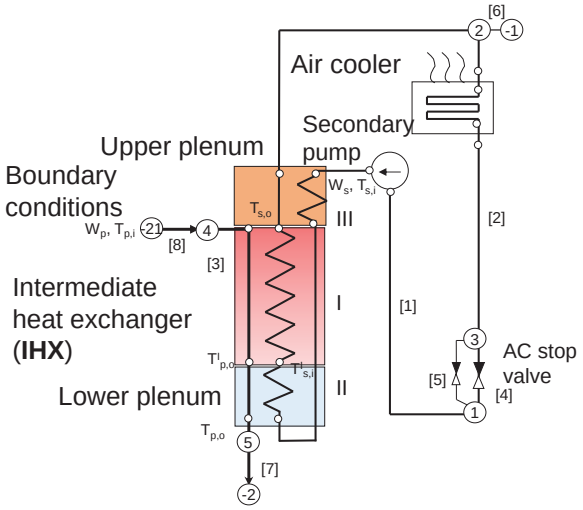

Figure 5. Calculation model of the IHX of "Monju".

Inlet conditions on the primary side are given to the code as boundary conditions, i.e., inlet flow rate and temperature. A constant pressure is given to the code as the outlet boundary condition. Regarding the secondary heat transport system, the flow rate is controlled by the pump and the temperature is controlled by the air cooler simulating the experimental conditions of "Monju" during the turbine trip test. In terms of the heat transfer coefficient, the correlation expressed in Eq. (2), i.e., Seban and Shimazaki correlation, is simply used for primary and secondary sides of these separated countercurrent-type heat exchangers. Although there are many kinds of heat transfer correlations on the shell side which were recently reviewed by Mikityuku [8], the same heat transfer coefficient as the heat transfer tube was used. Since flow rate is low, it was confirmed beforehand that the sensitivity of the correlations is very small.

3.2. Calculated Results

After the temperatures around the IHX are calculated using the system code, the heat transfer coefficients for the primary and the secondary are evaluated based on the theory of the countercurrent heat exchanger. Evaluated Nu numbers are shown in **Fig. 6** as a function of Pe number. The legend expressed with "p" stands for measured result on the primary side (shell) and with "s" stands for measured result on the secondary side (tube). While, calculated results are Nu numbers in tube. There is no data for "Monju" in low Pe number region because a special experiment like a natural circulation test was not conducted yet. Nevertheless the tendency of the heat transfer degradation is reproduced by implementing a separate heat exchanger model. This result indicates that the evaluated Nu number is a superficial one. Because real Nu number used for the calculation is expressed by Eq. (2). This discrepancy is definitely caused by the heat transfer other than the heat transfer tube region.

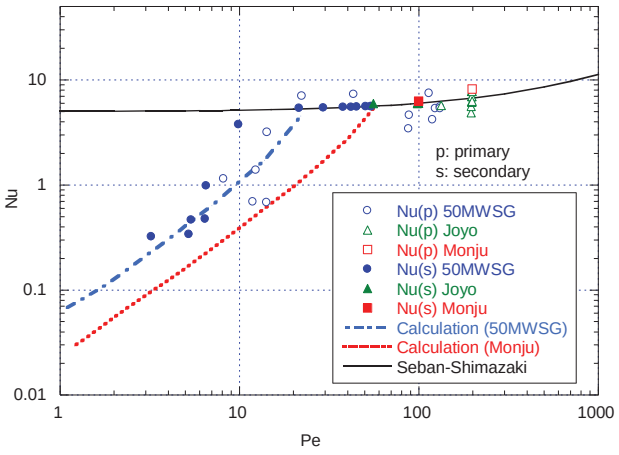

Figure 6. Comparison of Nu number between measurement and calculation based on the temperatures at inlet and outlet of IHX.

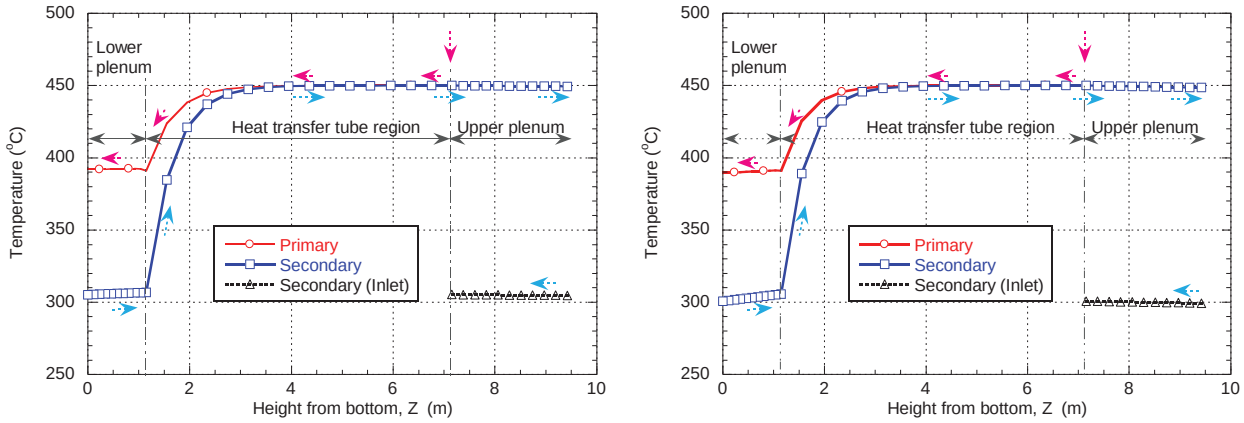

Figure 7. Temperature distribution in IHX in the case of low flow rate (left: 10% flow rate, right: 2.5% flow rate)

The Nu number for the 50MW SG is also calculated by changing dimensions of the IHX. The evaluated Nu number trances the measured result quantitatively. This result proves that the IHX should be divided into several heat exchangers in order to obtain good agreement in temperature distribution in the IHX under low flow rate conditions. **Figure 7** illustrates the temperature distribution in the IHX of "Monju". Arrows in this figure indicate the flow directions on both sides in the IHX. It seems that the temperature increase in the plenum is not very large even under the condition of 2.5% flow rate. However, the heat transfer in the lower plenum is considerable when we take into account the heat transfer area of the lower plenum which is approximately 1/100 of the heat transfer tube region.

4. DISCUSSION

As a result of two kinds of calculations, it is clarified that the degradation of the heat transfer coefficient measured by a countercurrent heat exchanger is a superficial phenomenon which is caused by heat transfer balance between the tube and the plenum regions. When the heat transfer coefficient is evaluated as one heat exchanger using Eq. (1)-(3), the heat transfer coefficient is degraded as flow rate decrease. However, the true heat transfer coefficient in the each part of the heat exchanger obeys an empirical correlation like the Seban & Shimazaki.

If heat transfer by fouling and the heat transfer in the upper plenum, i.e., heat exchanger III, in Fig. 5 are neglected, the heat transfer in the countercurrent heat exchanger should be calculated using the flowing equations;

$$Q = Q^I + Q^{II} = \frac{\Delta T_{l,m}^I}{R^I} + \frac{\Delta T_{l,m}^{II}}{R^{II}} \tag{9},$$

$$R^I = \frac{1}{\pi N L^I}\left(\frac{1}{d_o h_P^I} + \frac{1}{d_i h_s^I} + \frac{1}{2k_t^I}\ln\left(\frac{d_o^I}{d_i^I}\right)\right) \tag{10},$$

$$R^{II} = \frac{1}{\pi L^{II}}\left(\frac{1}{D_o h_p^{II}} + \frac{1}{D_i h_s^{II}} + \frac{1}{2k_t^{II}}\ln\left(\frac{D_o}{D_i}\right)\right) \tag{11},$$

$$\Delta T_{l,m}^I = \frac{\Delta T_1^I - \Delta T_2^I}{\ln\left(\frac{\Delta T_1^I}{\Delta T_2^I}\right)} = \frac{\left(T_{p,i} - T_{s,o}\right) - \left(T_{p,o}^I - T_{s,i}^I\right)}{\ln\left(\frac{T_{p,i} - T_{s,o}}{T_{p,o}^I - T_{s,i}^I}\right)} \tag{12},$$

$$\Delta T_{l,m}^{II} = \frac{\Delta T_1^{II} - \Delta T_2^{II}}{\ln\left(\frac{\Delta T_1^{II}}{\Delta T_2^{II}}\right)} = \frac{\left(T_{p,o}^I - T_{s,i}^I\right) - \left(T_{p,o} - T_{s,i}\right)}{\ln\left(\frac{T_{p,o}^I - T_{s,i}^I}{T_{p,o} - T_{s,i}}\right)} \tag{13},$$

$$Nu = \frac{h \cdot De}{k} \tag{14}.$$

where, super-scripts I and II denote the parameters in heat exchanger I and II, respectively. The logarithmic mean temperature difference $\Delta T_{l,m}^I$ decreases as flow rate decreases. Nevertheless, we used Eqs. (1) to (3) to evaluate the heat transfer coefficient. In this way, the logarithmic mean temperature difference has been overestimated and the heat transfer coefficient has been underestimated.

When we refer to the report of experiments by Johnson et al. [7] using lead-bismuth and mercury, the Nu number decreases in the similar manner as the present calculation. Their measured data are shown in **Fig. 8**. Other than their data, Subbotin's data are introduced in the data book by Nishio et al. [9]. The Nu number data were reproduced from the data book because his original data could not be found out in the paper with Subbotin's original data. The calculation results for the IHXs of "Monju" and 50MW SG are illustrated in the same figure. There are some offsets between the calculated results and data because of the differences of the experimental apparatuses with which the presentation calculates the heat transfer. However, trends of the heat transfer degradation are similar to those of the calculated results.

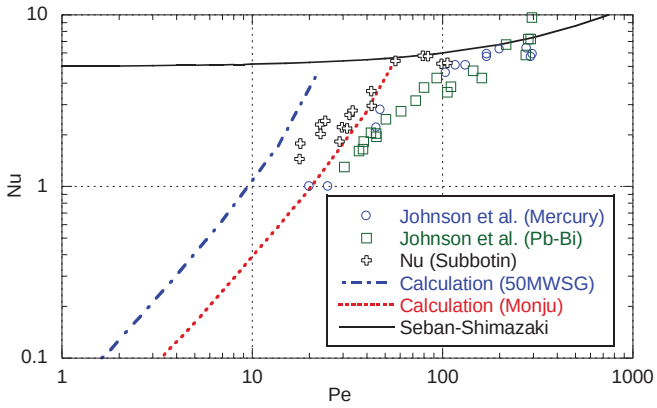

Figure 8. Comparison of Nu number between measurement and calculation.

Johnson et al. conducted their experiments using a set-up illustrated in **Fig. 9**. This drawing is reproduced from their original paper. When we look carefully into this drawing, temperature measurement points at the inlet and outlet of the set-up are not the exact locations of the heated section. I suspect that the heat input occurred by the pre-heaters in two regions between heated section and thermocouples. This might cause experimental errors resulting in the Nu number degradation in the low Pe number region as same as the case of the Nu number in IHX. In terms of the experiment by Subbotin, a schematic of the test section is illustrated in the paper by Subbotin [10], and supposedly a similar setup illustrated in **Fig. 10** was used in the measurement. This set-up had two plena where the heat transfer might occur at the inlet and outlet. The temperature between the inlet and the bottom of the heater was possibly increased by the heater wounded around the set-up. The degradation of the heat transfer coefficient might occur when temperature difference between outlet and inlet was overestimated, because the heat transfer coefficient *h* might be calculated using the following equation.

$$h = \frac{q}{\Delta T} = \frac{q}{\left(\Delta T_{test} + \Delta T_{in} + \Delta T_{out}\right)} \tag{15}$$

where, q stands for heat flux, and ΔT_{test}, ΔT_{in} and ΔT_{out} stand for temperature increases at the test section, inlet region and outlet region, respectively. Originally, ΔT_{in} and ΔT_{out} should have been zero in order to evaluate correct heat transfer coefficient. However, it is quite sure that temperature differences at the inlet and the outlet were not zero for their experimental set-ups because pre-heater wires give extra heat to liquid metal. The temperature increase was emphasized under the low flow rate conditions because the liquid metal stayed longer in the plena. Because of this situation, the heat transfer coefficient might be estimated as the flow rate decreased.

Finally the author would like to propose that the degraded data should not be referred in the evaluation. Especially for liquid metal reactors, since purity management is conducted completely, the correlation by Lubarsky and Kaufman is too conservative. Moreover, a heat exchanger should be divided into a couple of sections in a calculation even though the heat transfer area other than the heat transfer tube region seemed to be very small.

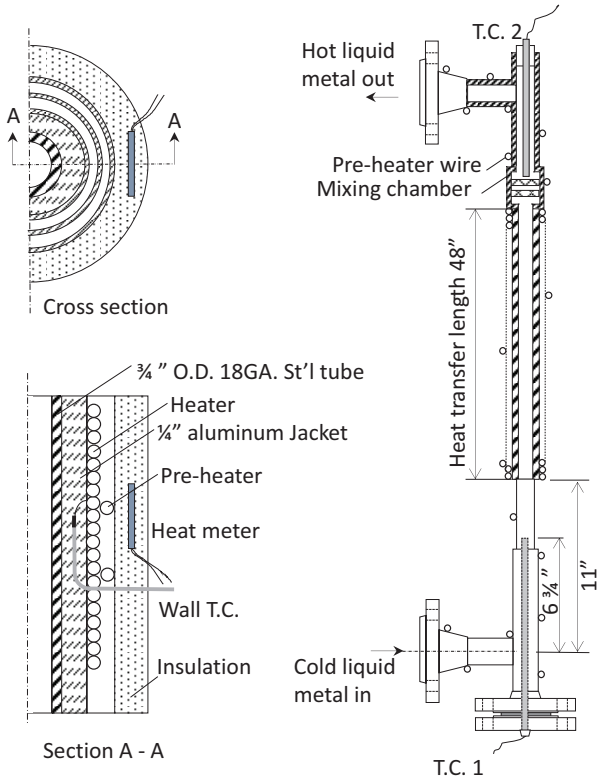

Figure 9. Experimental set-up of Johnson et al. [7].

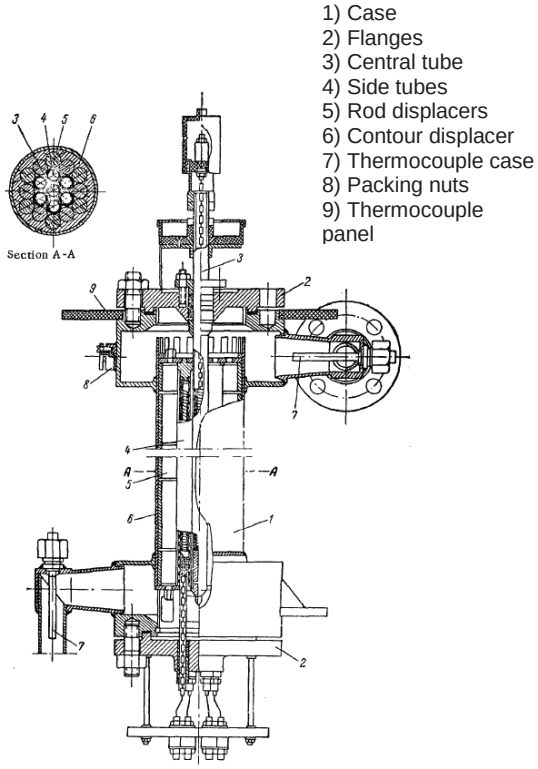

Figure 10. Experimental set-up of Subbotin et al. [10].

5. CONCLUSIONS

The thermal-hydraulics in an IHX of "Monju" reactor is calculated using CFD code. Inspired by the CFD calculation result, the thermal-hydraulics of IHXs for the "Monju" and 50MW SG Facility were calculated using the one-dimensional system code NETFLOW++. Through two kinds of investigations, the following results have been obtained.

(1) Since the Nusselt number is evaluated using inlet and outlet temperatures on the primary and the secondary sides of the heat exchange, a correct Nusselt number cannot be obtained if the heat transfers in the lower and the upper plena are taking into account.

(2) It is recommend that a calculation model of a heat exchanger is constructed as follows. One heat exchanger is divided into three heat exchangers, i.e., the heat transfer region, an upper plenum and a lower plenum, when the heat transfer under the low flow rate condition is calculated using a one-dimensional code. As for the heat transfer coefficient, we can use the empirical correlation such as the Seban and Shimazaki.

(3) The Nu number deviation from the theoretical value as a function of the Pe number under the low flow rate conditions can be predicted using the separate heat exchanger model.

(4) It has been concluded that the Nusselt number decrease for a countercurrent-type heat exchanger under low flow rate conditions is a superficial phenomenon.

(5) The Nu number in the literature showing degradation was possibly evaluated by inaccurate temperatures around the heat exchanger. Therefore, it would be better to neglect these data in future evaluation.

NOMENCLATURE

A: heat transfer area (m^2)
D: diameter of lower header inner shell
De: equivalent diameter (m)
d: diameter of heat transfer tube (m)
h: heat transfer coefficient (W/m^2K)
k: thermal conductivity of fluid (W/mK)
L: length of heat transfer tube (m)
m: mass flow rate (kg/s)
N: number of heat transfer tubes (-)
Nu: Nusselt number (-)
Pe: Péclet number (-)
Q: heat transfer rate (W)
q: heat flux (W/m^2)
R: thermal resistance (K/W)
T: temperature (K)
ΔT: temperature difference (K)
ΔT_{lm}: logarithmic mean temperature difference (K)

Subscript

f: fouling
i: inside
o: outside
p: primary
s: secondary
t: tube

ACKNOWLEDGEMENTS

The present study includes the result of "R&D Core Program for the Commercialization of Fast Breeder Reactor using 'Monju' " entrusted to University of Fukui by the Ministry of Education, Culture, Sports, Science and Technology of Japan (MEXT). The author appreciates his financial support. The author also appreciates the contribution in analyses by Mr. A. Okamoto, Mr. K. Hirai and Mr. M. Takano.

REFERENCES

[1] Lyon, R.N., Liquid metal heat-transfer coefficients, Chemical Engineering Progress, **47**, 2, pp.75-79 (1951).

[2] Seban, R.A., Shimazaki, T.T., Heat Transfer to a Fluid Flowing Turbulently in a Smooth Pipe with Walls at Constant Temperature, Trans. ASME, **73**, pp.803-809 (1951).

[3] Subbotin, V. I., Papovyants, A.K., Kirillov, P.L., Ivanovskii, N.N., A study of heat transfer to molten sodium in tubes, Soviet J. Atomic Energy, 13, 991-994 (1963), (translated from Atomnaya Énergiya, **13**, 4, pp.380-382 (1962)).

[4] Lubarsky, B., Kaufman, S.J., Review of Experimental Investigations of Liquid-Metal Heat Transfer, NACA TN 3336 (1955).

[5] Pacio, J., Marocco, L. and Wetzel, Th., Review of data and correlations for turbulent forced convective heat transfer of liquid metals in pipes, Heat Mass Transfer, Published on line, DOI 10.1007/s00231-014-1392-3 (2014).

[6] Mochizuki, H., Takano M., Heat transfer in heat exchangers of sodium cooled fast reactor systems, Nuclear Engineering and Design, **239**, pp.295-307 (2009).

[7] Johnson, H.A., Hartnett, J.P. and Clabaugh, W.J., Heat transfer to lead-bismuth and mercury in laminar and transitor pipe flow, Berkeley, California, United States Atomic Energy Commission AECU-2637 (1953).

[8] Mikityuk, K., Heat transfer to liquid metal: Review of data and correlations for tube bundles, Nuclear Engineering and Design, **239**, pp.680-687 (2009).

[9] Nishio, S., JSME Data Book Heat Transfer 5th Edition, Japan Society of Mechanical Engineers (2009).

[10] Subbotin, V.I., Ushakov, P.A. and Gabrianovich, B.N., Heat exchange during the flow of mercury and water in a tightly packed rod pile, Soviet J. Atomic Energy, **9**, pp.1001-1009 (1961), (translated from Atomnaya Énergiya, **9**, 6, pp.461-469 (1960)).